Article

Improved Corrosion Protection of Acrylic Waterborne Coating by Doping with Microencapsulated Corrosion Inhibitors

Jacob Ress, Ulises Martin and David M. Bastidas *

National Center for Education and Research on Corrosion and Materials Performance, NCERCAMP-UA, Department of the Chemical, Biomolecular and Corrosion Engineering, The University of Akron, 302 E Buchtel Ave, Akron, OH 44325–3906, USA; jtr45@uakron.edu (J.R.); um11@uakron.edu (U.M.)
* Correspondence: dbastidas@uakron.edu; Tel.: +1-330-972-2968

Abstract: Herein, a waterborne acrylic coating doped with pH sensitive colophony microcapsules containing corrosion inhibitors was studied on carbon steel plates. The changes in the physical properties of the coatings were studied. The microcapsule coating specimens maintained more noble E_{corr} values compared to the control in deionized water and simulated concrete pore solutions with -513 and -531 mV_{SCE}, respectively. Additionally, the microcapsule polarization results for both pH 12.6 and 6.2 electrolyte solutions showed lower i_{corr} values of 1.20×10^{-6} and 3.24×10^{-6} $A \cdot cm^{-2}$, respectively, compared to the control sample (1.15×10^{-5} and 4.21×10^{-5} $A \cdot cm^{-2}$). Therefore, the microcapsule coating provided more protection from chloride attack on the substrate as well as the deleterious effects of low pH on carbon steel. The electrochemical impedance spectroscopy analysis corroborated the DC polarization results, showing increased corrosion resistance for the microcapsule coated specimens compared to the control. Moreover, the R_{pore} and R_{ct} are much higher than the control, indicating the protection of the inhibitors. The $C_{eff,dl}$ also shows lower values for the microcapsule coating than the control, showing a more protective and less doped double layer.

Keywords: smart corrosion inhibitors; acrylic coating; simulated concrete pore solution; microcapsules; chlorides; double-emulsion

1. Introduction

The corrosion of steel reinforced concrete has been a source of significant economic loss in the construction and transportation industry [1]. Therefore, the use of physical barriers has been used to deter the corrosion process, such as the use of coatings [2–4]. The use of coatings in reinforced concrete structures has been widely studied for its corrosion protection in mortar as well as simulated concrete pore solution (SCPS) [5,6]. The most common coating type for the reinforced concrete application is the use of an epoxy coating, due to its very low porosity, increased hardness, and offered protection against chlorides and other corrosive agents [7]. However, epoxy coatings can present a large cost and long drying periods whereas acrylic coatings can provide a faster drying, cheaper solution.

Due to the amount of volatile organic compounds (VOCs) and the harmful environmental effects they impart, the use of waterborne coatings has been an attractive area of study in recent years [8]. In waterborne coatings, acrylics are the most often used binder resin [9]. They present a viable alternative to solvent-based coatings which contain volatile organic compound (VOC) that negatively affect the environment [10]. The use of functionalized waterborne acrylic (WA) coatings has been of particular interest. In the works of Ecco et al. and González et al., CeO nanoparticles were incorporated in the WA coatings which improved the corrosion resistance significantly [11,12]. Similarly, the use of a WA coating with phosphate functionalities has been shown to be able to phosphatize the metal surface using a thin coating containing functional nanoparticles [13]. However, WA coatings are not without drawbacks, Dogen-Guner et al. used cellulose nanocrystals to enhance the mechanical properties of WA coatings without the use of added coalescents, which

often add VOCs to plasticize the particles to enable film formation [9]. In the work of Ni et al., poly(styrene-acrolein)/reduced graphene oxide nanocomposites were synthesized to disperse corrosion inhibiting graphene oxide to improve the corrosion resistance given by the coating [10]. The nanocomposites proved to be effective at enhancing the anticorrosion properties of the coating, however, their fabrication may prove to present difficulties when considering costs and scalability.

In recent years, the use of microcapsules containing active agents has been of particular interest for the applications of self-healing and corrosion resistance. In the work of Zhang et al., self-healing microcapsules were synthesized for implementation to waterborne epoxy coatings [14]. Bao et al. synthesized microcapsules from ZnO and benzotriazole (BTA) in a simple one-step method to increase corrosion protection in waterborne polyacrylate coatings [15]. Smart microcapsules which can release the active agents in response to certain chemical, mechanical, or other triggers have been particularly of interest in recent coating technologies. An anticorrosion coating containing self-repairing polyurea-formaldehyde microcapsules was developed by Njoku et al. to protect aluminum alloy 2024 [16]. The microcapsules respond to changes in pH or chloride ion concentration, dissolving the shell and allowing the diffusion of corrosion inhibitors.

Similarly, microcapsules made by the double emulsion method have been developed by the authors [17]. The microcapsule shell is composed of colophony (>99% abietic acid) containing $NaNO_2$ corrosion inhibitors. $NaNO_2$ was used due to its excellent performance in concrete environments, in which it can prevent corrosion caused by chloride and carbonation while having good compatibility with concrete [18,19]. The nitrite ions facilitate the formation of stable Fe_2O_3 and γ-FeOOH in the passive film, protecting the rebar [20]. It was found that, in alkaline solution, the abietic acid shell deprotonates and the shell becomes porous, allowing for the diffusion of the corrosion inhibitor. Furthermore, previous research of colophony in concrete environments showed increased mechanical properties and a decrease in the porosity of the concrete [21]. In this work, a commercial WA coating was doped with colophony microcapsules (MC) containing $NaNO_2$ corrosion inhibitors. The MC coating was then characterized by SEM, water absorption, infinite focus microscope (IFM), and thermal gravimetric analysis (TGA) and compared to the base WA coating. The anticorrosion properties were measured using electrochemical impedance spectroscopy (EIS) and potentiodynamic polarization.

2. Materials and Methods

Colophony microcapsules were synthesized according to the protocol previously described by the author with modified stirring speeds. First, ground colophony powder was dissolved in diethyl ether. Then, an aqueous solution of 1.5 M $NaNO_2$ and 1 wt% polyvinyl alcohol (PVA) was added dropwise while stirring with an overhead stirrer at a rate of 550 rpm for 4 min. An aqueous solution of 4 wt% PVA was added under reduced stirring of 350 rpm to create the water-in-oil-in-water double emulsion [22,23]. Lastly, the remaining organic solvent was evaporated by heating at 60 °C for 2 h. The microcapsules were filtered and washed using deionized (DI) water before direct addition to the coating. Carbon steel panels with composition shown in Table 1 as-received from the Q-lab were coated with WA coating, using a drawdown bar, with and without colophony microcapsules with a wet thickness of 50 μm.

Table 1. The composition of carbon steel specimens (wt%).

C	Mn	P	S	Si	Cu	Ni	Cr	Mo	V	Fe
0.28	1.08	0.019	0.043	0.20	0.37	0.16	0.16	0.050	0.0379	Bal.

The WA coating used was commercially available with composition as shown in Table 2. The coating was left to dry in air for 24 h. The microcapsules were added to the coating before application at a concentration of 50 g/L. Control samples of acrylic

coating were prepared for comparison of corrosion performance. The water uptake was determined by gravimetric analysis over a period of 30 days and performed in triplicate. The acrylic coatings with and without MCs were exposed to DI water and the mass change was measured. The specimens were lightly dried by light dabbing before weighing.

Table 2. Composition of waterborne acrylic coating (wt%).

TiO	Propylene Glycol	Alumina	Hydrated Aluminum Magnesium Silicate	Lithium Hydroxide Monohydrate	Acrylic Polymer Emulsion
20.0	10.0	2.0	1.0	<0.1	Bal.

The size and morphology of the microcapsules were analyzed by scanning electronic microscopy (SEM, Hitachi High-Tech America Inc., Schaumburg, IL, USA) using a Hitachi TM 3030+ SEM and back scattered electron (BSE, Hitachi High-Tech America Inc., Schaumburg, IL, USA) technique with an excitation signal of 15 kV and 8 μm working distance. Energy dispersive X-ray (EDX, Hitachi High-Tech America Inc., Schaumburg, IL, USA) analysis was also performed on the coating with and without microcapsules to determine the surface atomic composition.

The corrosion performance of the coating was tested using a Gamry series 600 potentiostat (Gamry Instruments, Warminster, PA, USA) with a three-electrode set up: a saturated calomel electrode as reference, a graphite rod as the counter electrode, and carbon steel Q-panels 3×6 in with coating as the working electrode. The experiments were conducted in 3.5 wt% NaCl solution in DI water with pH 6.8 and simulated concrete pore solution (SCPS) composed of saturated $Ca(OH)_2$ with pH 12.6. First, open circuit potential was obtained over 1 h to determine the stable steady-state potential. Then, electrochemical impedance spectroscopy (EIS) was performed at OCP using 10 mV r.m.s. with 10 points/decade, scanning the frequencies between 10^5 and 10^{-2} Hz. Finally, potentiodynamic polarization scans were performed from -0.2 to $+0.2$ V_{OCP} to determine the Tafel slopes and calculate the corrosion current density (i_{corr}). All tests were performed in triplicate to ensure reproducibility.

3. Results

The colophony microcapsules are shown in Figure 1. The larger microcapsules are around 50 μm in diameter, with smaller ones measuring less than 10 μm. The average size of the microcapsules used for the coatings was found to be 42 μm. The microcapsules are spherical in morphology with the appearance of pores on the surface, which appear due to the partial dissolution of colophony in solution, as well as drying of the microcapsules as the solution inside evaporates [22]. Moreover, the microcapsules show agglomeration when drying as the abietic acids attract each other from the oppositely charged ends [24].

The coated steel specimens imaged by SEM are shown in Figure 2, which shows the control WA coating and the MC doped WA coating. In both coatings, cracks are observed with small dimples. These areas can be the cause of corrosion initiation due to the ingress of water and aggressive ion, diffusing to the steel substrate and initiating iron acid hydrolysis [18]. In the MC doped sample, the larger microcapsules can be seen by the bumps on the surface.
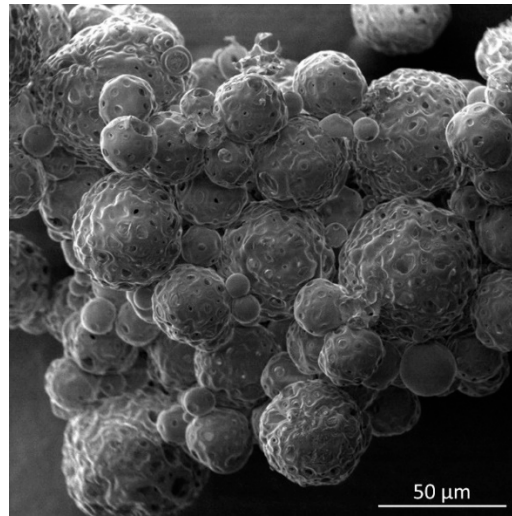
Figure 1. SEM micrograph of colophony microcapsules added to modify the acrylic coating.
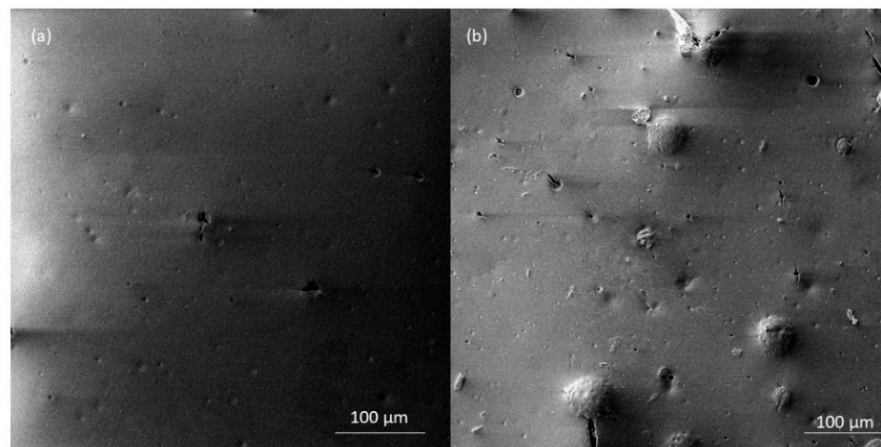

Figure 2. SEM images of (**a**) acrylic coating control sample, and (**b**) acrylic coating doped with colophony microcapsules.

The surface of the coated carbon steel sheets was investigated using IFM, shown in Figure 3. The control sample containing no microcapsules shows the roughness of the coating with 30 μm. The MC coating specimens, however, display a larger roughness due to the elevated portions around the microcapsules. The large singular microcapsules and clusters can be observed by the areas in the yellow to orange range (20–30 μm), and between these sections, the same surface roughness as the control can be observed. Overall, the MC coating specimens cause an increase in height difference of almost double.

Figure 4 shows the water uptake for the control and MC specimen over a 30-day test period. The water uptake tests were performed in triplicate and the error bars represent the standard deviation. The MC specimen showed increased water absorption compared to the control, however it remained under 0.6% throughout the test duration. The MC specimen contained colophony has hydroxyl groups, thus making water permeation into the coating easier [24]. Additionally, the increased roughness of the coating surface for the MC specimens may have led to increased entrapment of water, thus increasing the measured water absorption. The higher water absorption shown by the MC samples benefits the coating as the water allows the inhibitors to diffuse from the MCs. The inhibitors, when in contact with the steel substrate can then form a passive oxide layer to protect the steel from iron acid hydrolysis [18].
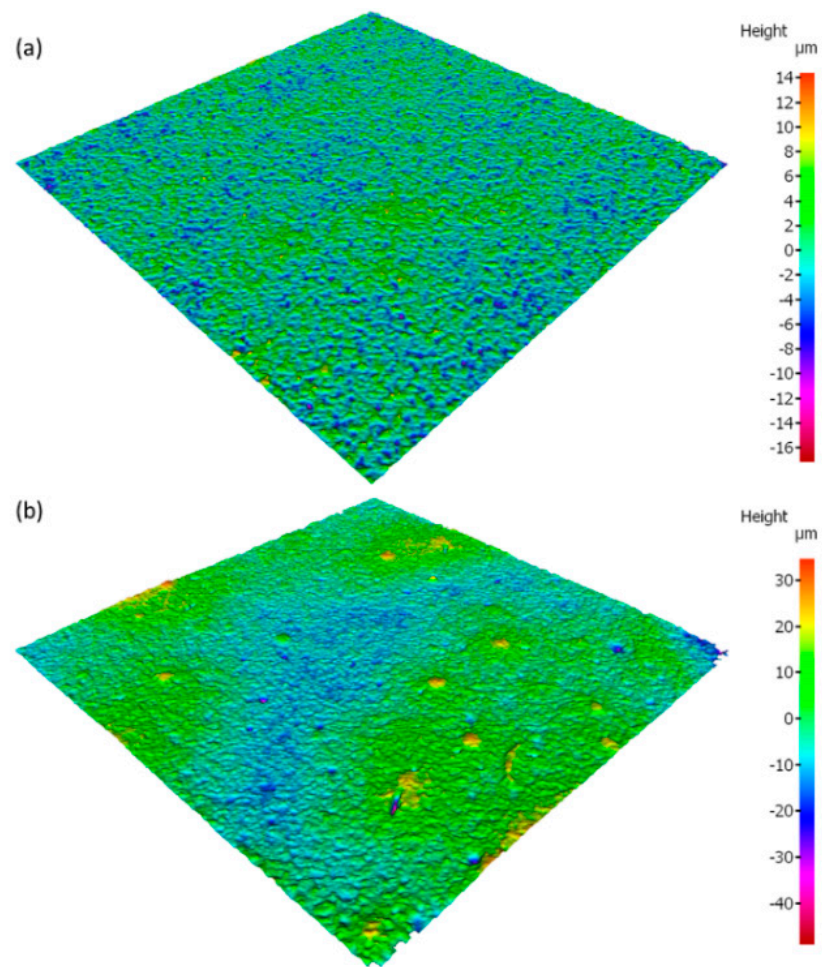
Figure 3. Infinite focus micrographs for (**a**) acrylic coating, and (**b**) acrylic coating containing microcapsules.
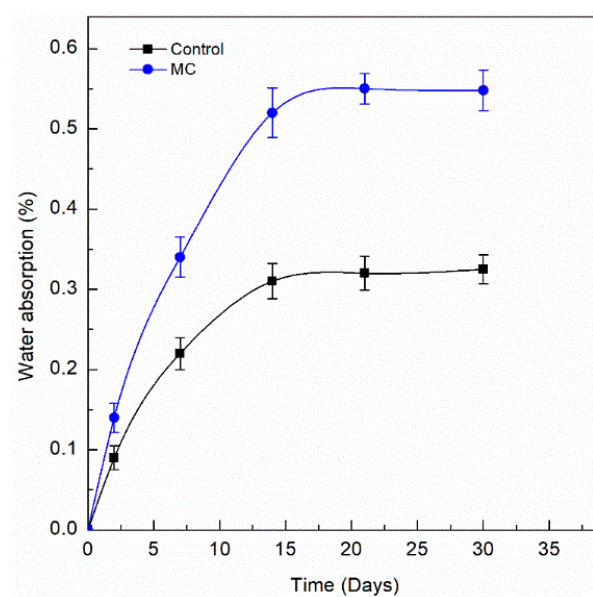

Figure 4. The water uptake of coatings with microcapsules (MC) and without microcapsules (control) on carbon steel plates measured by gravimetric analysis. Error bars represent the standard deviation.

The thermal stability of the coating and the MC doped coating were examined using TGA analysis. Figure 5 shows the weight loss curves for both specimens. The test was performed in duplicate to ensure reproducibility. The control specimen maintains stability, showing very little weight loss, for temperatures up to around 300 °C. After this point, the coating degrades up to 700 °C, showing nearly 60% weight loss. The MC coating shows an earlier decomposition, beginning below 200 °C. Additionally, the MC coating shows a higher weight loss due to water evaporation, because of the increased amount of water from the MC addition. Both samples exhibit the major mass loss event around 300 °C due to the coating decomposition, however the MC coating shows a steeper decline. This initial mass loss is due to the evaporation of moisture from the microcapsules as well as degradation of the microcapsules, shown in a previous study [17]. Additionally, the MC specimen shows a slightly greater mass loss overall, however it is comparable to the control at 700 °C. This shows that the MC coating exhibits less thermal stability compared to the control due to the nature of the microcapsules present in the coating.
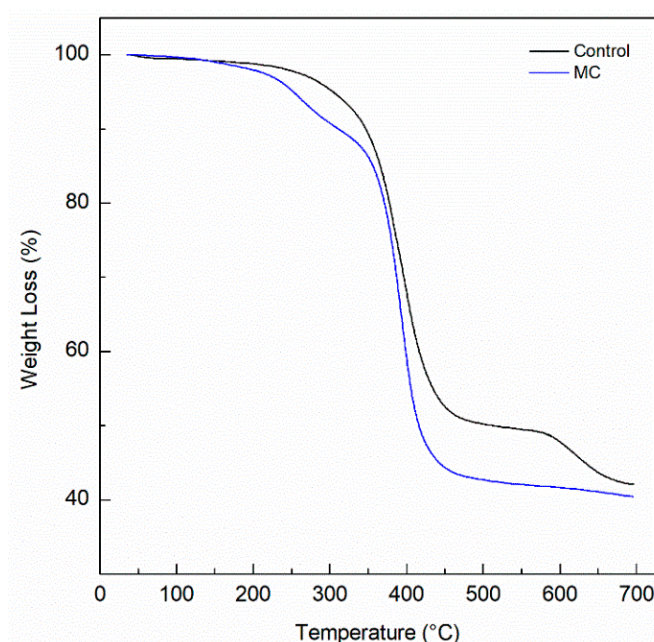

Figure 5. TGA curves for the WA coating control and WA coating doped with colophony microcapsules.

The increased corrosion protection of the MC coating was tested, and the polarization curves obtained are shown in Figure 6. In both DI and SCPS solution with 3.5 wt% NaCl, the MC coating showed more noble corrosion potential (E_{corr}) values with -532 and -513 mV$_{SCE}$, respectively. Additionally, the corrosion current density (i_{corr}) values were calculated by Tafel analysis and are shown in Table 3. For the DI condition, the MC coating measured an i_{corr} of 1.20×10^{-6} A/cm^2, nearly one order of magnitude lower than the control sample, thus much lower corrosion. The blank sample with no coating showed the most active i_{corr} with a similar E_{corr} to the control coating. Moreover, the anodic Tafel slope, β_a, showed a decrease from the control, thus the kinetics of the anodic reaction of elemental Fe oxidizing to Fe^{2+} had decreased. The cathodic slope, β_c, however showed an increase when the microcapsules were present, this is likely due to the reaction of the colophony with oxygen, as the oxidation of colophony has been previously studied in air and in aqueous solutions [25]. Therefore, the kinetics of the cathodic reaction, oxygen reduction, increased. The same trend for i_{corr} and the Tafel slopes can be seen in the SCPS solution. Overall, the corrosion parameters decreased due to the alkalinity of the solution, pH 12.6, and the carbon steel spontaneously forms a passive film of lepidocrocite and magnetite, γ-FeOOH and Fe$_3$O$_4$, respectively [18]. Due to this, the MC coating shows the lowest i_{corr} and

the most noble E_{corr} with 1.20×10^{-6} A/cm^2 and -513 mV$_{SCE}$, respectively. Both E_{corr} and i_{corr} values obtained for the MC coating show improved corrosion performance compared to the modified acrylic coating of Gao et al., whose polarization results demonstrated E_{corr} values below -500 mV$_{SCE}$ and i_{corr} values around 1×10^{-4} A/cm^2 [26].
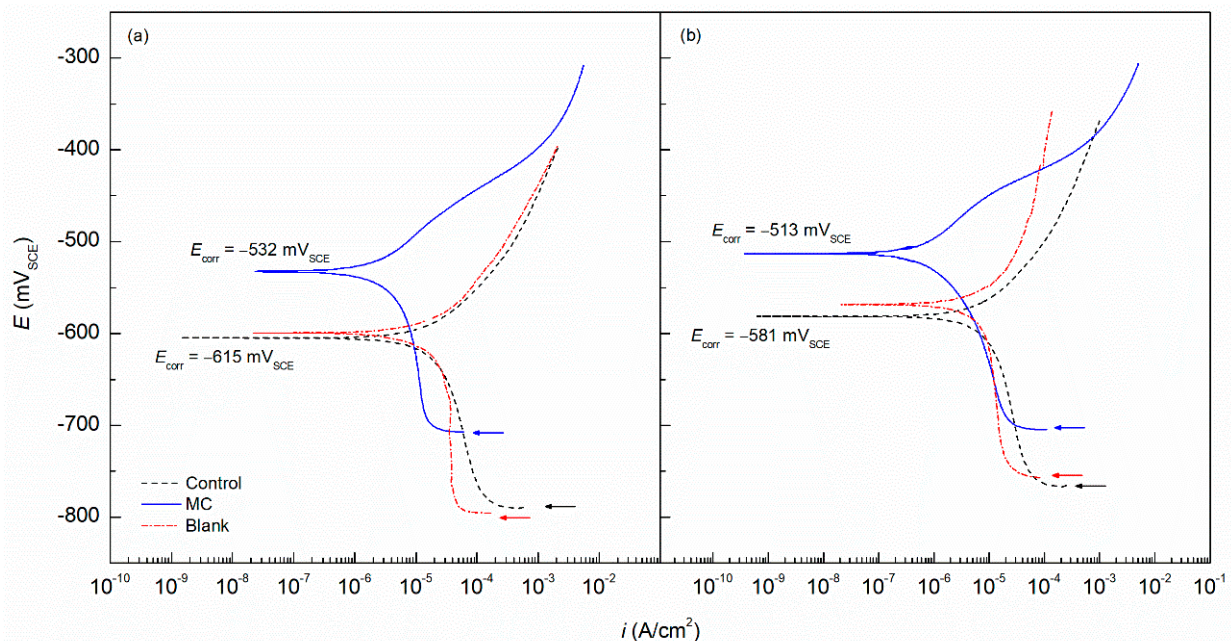

Figure 6. Potentiodynamic polarization curves for mild steel with acrylic coating modified with colophony microcapsules exposed to 3.5 wt% NaCl in (**a**) DI water (pH = 6.8) and (**b**) SCPS (pH = 12.6).

Table 3. Electrochemical parameters calculated by Tafel fitting from potentiodynamic polarization for acrylic coating containing microcapsules exposed to 3.5 wt% NaCl contaminated environment in DI water (pH 6.8) and SCPS (pH 12.6). The standard deviation is presented in the parenthesis.

pH	Sample	E_{corr} (mV$_{SCE}$)	i_{corr} (A/cm^2)	βa (mV/dec)	βc (mV/dec)
	MC	-532 (±21)	3.24×10^{-6} ($\pm1.24 \times 10^{-6}$)	68 (±11)	143 (±21)
6.8	Control	-615 (±15)	4.21×10^{-5} ($\pm1.94 \times 10^{-6}$)	63 (±9)	365 (±35)
	Blank	-599 (±13)	6.89×10^{-5} ($\pm2.67 \times 10^{-5}$)	65 (±14)	221 (±17)
	MC	-513 (±10)	1.20×10^{-6} ($\pm2.29 \times 10^{-6}$)	95 (±10)	119 (±13)
12.6	Control	-581 (±18)	1.15×10^{-5} ($\pm3.04 \times 10^{-6}$)	84 (±14)	275 (±25)
	Blank	-568 (±22)	1.59×10^{-5} ($\pm1.55 \times 10^{-5}$)	96 (±17)	253 (±22)

In addition to polarization scans, EIS was conducted to determine the resistances and capacitances of the interfaces in the system. Figure 7 shows the Nyquist plots for the control and MC doped specimens in DI and SCPS contaminated with 3.5 wt% NaCl as well as a bare steel sample labeled as blank.

It can be seen in both solutions that the MC specimens provide increased impedance values compared to the control. Overall, the measurements in DI show decreased impedance compared to SCPS, this is due to the lower pH hindering the formation of the passive oxide film [27,28]. The depressed semicircles for the DI show the MC specimen reaching over 2 kΩ·cm^2 while the control shows only 1 kΩ·cm^2. The SCPS specimens, however showed increases in impedance with nearly 2.75 and 1.5 kΩ·cm^2 for the MC and control specimen, respectively. The EIS data was fit to an electrical equivalent circuit (EEC) shown in Figure 8, with R_s for the solution resistance and two time constants, including two relaxation processes, a R_{pore}–CPE_{pore} to represent the pores in the coating, and R_{ct}–CPE_{dl} to represent the corrosion process.
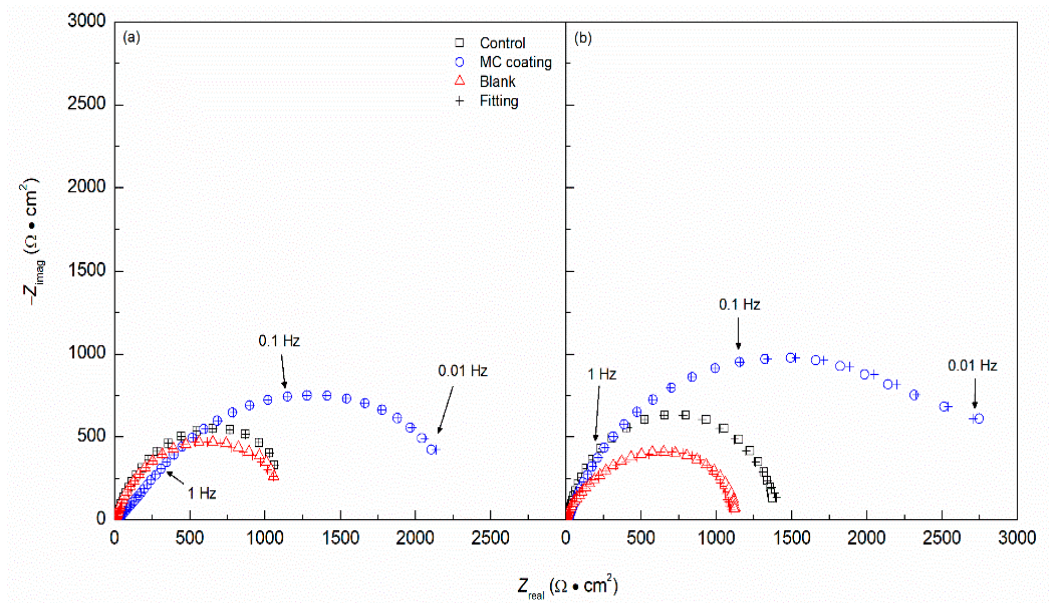
Figure 7. Nyquist plots obtained from EIS for mild steel with acrylic coating modified with colophony microcapsules exposed to 3.5 wt% NaCl in (**a**) DI water (pH = 6.8), and (**b**) SCPS (pH = 12.6).
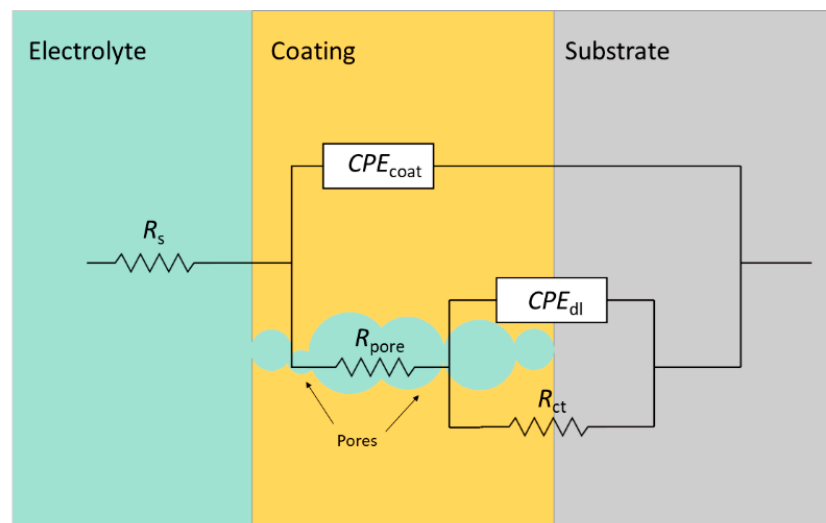

Figure 8. The electrical equivalent circuit (EEC) used to model the EIS data for the MC coating and the control coating.

The EEC fitting parameters are shown in Table 4. The solution resistance, R_s, was measured to be about 17 $\Omega \cdot cm^2$ for the SCPS solution and 19–24 $\Omega \cdot cm^2$ for the DI solution. The increased resistance for the DI solution is due to the lower concentration of ions. SCPS contains a higher concentration of Ca^{2+} and OH^- ions, making the solution more conductive and R_s lower. The improved corrosion resistance provided by the MC coating can be seen in both the pore resistance, R_{pore}, and the charge transfer resistance, R_{ct}, in both solutions. The DI control coating shows a R_{pore} value of 286 $\Omega \cdot cm^2$ while the MC coating measures over twice the value with 609 $\Omega \cdot cm^2$, due to the existence of the corrosion inhibitors and the colophony microcapsules. The lowest performance is shown by the blank sample, corroborated by the DC results in the polarization curve. As shown by the polarization results, the cathodic corrosion inhibition shown by the increased cathodic Tafel slope in the presence of microcapsules slows the oxygen reduction kinetics, therefore, despite displaying a higher water absorption, the microcapsules improve the coating through the effects of the inhibitor compounds. The SCPS solution displays the same trend

with 195 and 280 $\Omega \cdot \text{cm}^2$ for the control and MC specimen, respectively. Furthermore, the R_{ct} values confirm the protection by the microcapsules. Both the SPCS and DI conditions show the MC specimens offering nearly twice the resistance and relatively close in value with 2.31×10^3 and 2.19×10^3 $\Omega \cdot \text{cm}^2$, respectively. Constant phase elements, *CPE*, are used in the EEC due to the nonideal capacitance shown by the interfaces. The capacitance given by the coating, CPE_{coat}, shows similar values for both the control and MC coating specimens, this is due to the similar coating thicknesses and protection offered by the film. The Y_{dl} values were used to calculate the effective capacitance for the double layer ($C_{\text{eff,dl}}$) according to Brug et al., see Equation (1) [29].

$$C_{\text{eff,dl}} = Y_{dl}^{1/n_{dl}} \left(\frac{1}{R_s} - \frac{1}{R_{ct}} \right)^{(n_{dl}-1)/n_{dl}} \tag{1}$$

where Y_{dl} is the admittance for the double layer and n_{dl} is the fractional power of the frequency for the double layer. In SCPS, the $C_{\text{eff,dl}}$ values for the MC sample show lower capacitance than the control with 1.82 $\mu\text{F}\cdot\text{cm}^{-2}$, due to the presence of microcapsules and inhibitors. The pH effect on the capacitance can be seen by the much higher $C_{\text{eff,dl}}$ values for the DI specimens. The MC specimen shows 2.26 $\mu\text{F}\cdot\text{cm}^{-2}$, higher than the control in SCPS. However, this remains lower than the control specimen in DI with 3.03 $\mu\text{F}\cdot\text{cm}^{-2}$, further indicating the protection afforded to the substrate by the MC doped coating. The impedance values shown by the MC coating are in agreement with the results obtained by Gao et al. and Lewis et al., which studied modified WA coating, finding improved corrosion resistance with their modified coating on the magnitude of 10^3 and 10^4 $\Omega \cdot \text{cm}^2$ [26,30].

Figure 9 shows an MC coating specimen with a large microcapsule at the center. The bump created by the microcapsule can be seen with small pores around its shell through the coating. These pores allow the $NaNO_2$ inhibitors to release, thus protecting the rebar which has become exposed due to the cracks that can be seen in Figure 2. This further explains the improved corrosion resistance seen in the MC coating specimens compared to the control sample coating. Due to the presence of these pores along with the increased corrosion protection from the MC specimens, the increased water absorption exhibited by the MC doped coating does not hinder the anticorrosion properties imparted by the microcapsules and corrosion inhibitors and the overall corrosion resistance is improved.
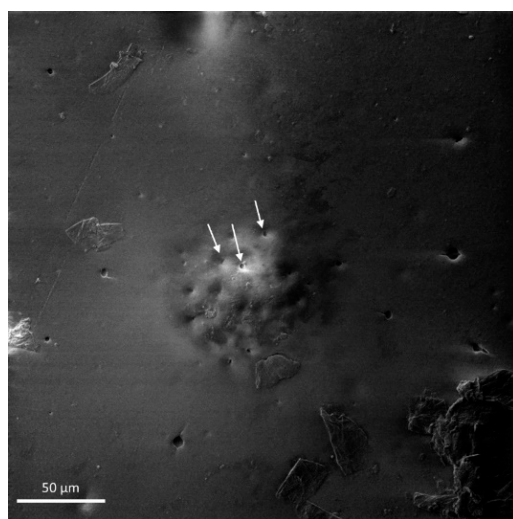

Figure 9. MC coating with a large microcapsule pictured in the center after electrochemical testing in SCPS. Arrows indicate pores from the microcapsules.

Table 4. EIS fitting values obtained for acrylic coated control steel panels and MC modified acrylic coated panels exposed to 3.5 wt% NaCl contaminated environment in DI water (pH 6.8) and SCPS (pH 12.6) using the equivalent circuit presented in Figure 8. The standard deviation is presented in the parenthesis.

pH	Sample	R_s ($\Omega \cdot cm^2$)	R_{pore} ($\Omega \cdot cm^2$)	Y_{coat} ($S \cdot cm^{-2} \cdot S^{n_{coat}}$)	n_{coat}	R_{ct} ($\Omega \cdot cm^2$)	Y_{dl} ($S \cdot cm^{-2} \cdot S^{n_{dl}}$)	n_{dl}	$C_{eff,dl}$ ($F \cdot cm^{-2}$)	χ^2
6.8	Control	19 ($\pm$5)	195 ($\pm$21)	1.18×10^{-4} ($\pm 4.4 \times 10^{-4}$)	0.84	1.22×10^3 ($\pm 1.1 \times 10^2$)	8.05×10^{-6} ($\pm 2.1 \times 10^{-6}$)	0.90	3.03×10^{-6}	1.77×10^{-4}
	MC	24 ($\pm$3)	280 ($\pm$28)	4.85×10^{-4} ($\pm 3.5 \times 10^{-4}$)	0.73	2.19×10^3 ($\pm 1.8 \times 10^2$)	3.47×10^{-6} ($\pm 1.6 \times 10^{-6}$)	0.91	2.26×10^{-6}	2.51×10^{-4}
	Blank	9 ($\pm$2)	–	–	–	1.01×10^3 ($\pm 2.4 \times 10^2$)	6.84×10^{-4} ($\pm 2.6 \times 10^{-4}$)	0.89	359×10^{-6}	9.23×10^{-4}
12.6	Control	17 ($\pm$2)	286 ($\pm$19)	9.88×10^{-4} ($\pm 3.0 \times 10^{-4}$)	0.91	1.41×10^3 ($\pm 0.5 \times 10^2$)	2.20×10^{-6} ($\pm 1.5 \times 10^{-6}$)	0.90	2.24×10^{-6}	2.93×10^{-4}
	MC	16 ($\pm$2)	609 ($\pm$25)	7.90×10^{-4} ($\pm 2.7 \times 10^{-4}$)	0.76	2.61×10^3 ($\pm 1.4 \times 10^2$)	4.21×10^{-6} ($\pm 1.8 \times 10^{-6}$)	0.92	1.82×10^{-6}	7.67×10^{-4}
	Blank	8 ($\pm$3)	–	–	–	1.12×10^3 ($\pm 2.3 \times 10^2$)	1.05×10^{-4} ($\pm 1.0 \times 10^{-4}$)	0.92	281×10^{-6}	3.89×10^{-4}

4. Conclusions

A waterborne acrylic coating doped with pH sensitive colophony microcapsules containing corrosion inhibitors was studied on carbon steel plates. The changes in the physical properties of the coatings were studied. Additionally, the coating was tested under accelerated corrosion conditions in DI and simulated concrete pore solutions contaminated with chloride. The following conclusions can be drawn.

- The addition of microcapsules to the coating increased the coating roughness, however the appearance of cracks did not change significantly. In a thin coating of 50 μm thickness, the larger microcapsules can be seen on the coating surface.
- The water absorption of the MC doped coating showed increased values compared to the control coating of nearly double. This is accounted for by the increased number of pores present in the coating after exposure to test media, due to the colophony microcapsule release mechanism.
- The thermal stability of the coating did not change significantly, however the degradation of the microcapsules occurs near 200 °C, before the coating begins to degrade around 300 °C.
- The MC coating specimens maintained more noble E_{corr} values compared to the control in DI and SCPS solutions with -532 and -513 mV$_{SCE}$, respectively. Additionally, the MC polarization results showed lower i_{corr} values by nearly one order of magnitude for both conditions. Therefore, the MC coating provided more protection from chloride attack on the substrate as well as the deleterious effects of low pH on carbon steel.
- The EIS analysis corroborated the DC polarization results, showing increased corrosion resistance for the MC coated specimens compared to the control. Moreover, the R_{pore} and R_{ct} are much higher than the control, indicating the protection of the inhibitors. The $C_{eff,dl}$ also shows lower values for the MC coating than the control, showing a more protective and less doped double layer.

Author Contributions: Conceptualization, D.M.B.; methodology, J.R., U.M. and D.M.B.; formal analysis, J.R., U.M. and D.M.B.; investigation, J.R., U.M. and D.M.B.; resources, D.M.B.; data curation, J.R., U.M. and D.M.B.; writing—original draft preparation, J.R., U.M. and D.M.B.; writing—review and editing, J.R. and D.M.B.; visualization, D.M.B.; supervision, D.M.B.; project administration, D.M.B.; funding acquisition, D.M.B. All authors have read and agreed to the published version of the manuscript.

Institutional Review Board Statement: Not applicable.

Informed Consent Statement: Not applicable.

Data Availability Statement: The raw/processed data required to reproduce these findings cannot be shared at this time as the data also forms part of an ongoing study.

Conflicts of Interest: The authors declare no conflict of interest.

References

1. Morris, W.; Vico, A.; Vázquez, M. Chloride induced corrosion of reinforcing steel evaluated by concrete resistivity measurements. *Electrochim. Acta* **2004**, *49*, 4447–4453. [CrossRef]
2. Qu, L.; Wang, Q.; Xu, S.; Wang, N.; Shi, Z. Chloride corrosion resistance of double-layer anticorrosive coating in simulated concrete pore solution. *Constr. Build. Mater.* **2021**, *295*, 123682. [CrossRef]
3. Afshar, A.; Jahandari, S.; Rasekh, H.; Shariati, M.; Afshar, A.; Shokrgozar, A. Corrosion resistance evaluation of rebars with various primers and coatings in concrete modified with different additives. *Constr. Build. Mater.* **2020**, *262*, 120034. [CrossRef]

4. Ress, J.; Martin, U.; Bosch, J.; Bastidas, D.M. Protection of carbon steel rebars by epoxy coating with smart environmentally friendly microcapsules. *Coatings* **2021**, *11*, 113. [CrossRef]
5. Nguyen, T.H.; Nguyen, T.A. Protection of steel rebar in salt-contaminated cement mortar using epoxy nanocomposite coatings. *Int. J. Electrochem.* **2018**, *2018*, 8386426. [CrossRef]
6. Liu, W.; Li, J.; Huang, X.; Bi, J. Corrosion protection of Q235 steel using epoxy coatings loaded with calcium carbonate microparticles modified by sodium lignosulfonate in simulated concrete pore solutions. *Materials* **2021**, *14*, 1982. [CrossRef]
7. Erdoğdu, Ş.; Bremner, T.W.; Kondratova, I.L. Accelerated testing of plain and epoxy-coated reinforcement in simulated seawater and chloride solutions. *Cem. Concr. Res.* **2001**, *31*, 861–867. [CrossRef]
8. Hettiarachchi, N.M.; De Silva, R.T.; Prasanga Gayanath Mantilaka, M.M.M.G.; Pasbakhsh, P.; De Silva, K.M.N.; Amaratunga, G.A.J. Synthesis of calcium carbonate microcapsules as self-healing containers. *RSC Adv.* **2019**, *9*, 23666–23677. [CrossRef]
9. Dogan-Guner, E.M.; Brownell, S.; Schueneman, G.T.; Shofner, M.L.; Meredith, J.C. Enabling zero added-coalescent waterborne acrylic coatings with cellulose nanocrystals. *Prog. Org. Coat.* **2021**, *150*, 105969. [CrossRef]
10. Jiao, C.; Sun, L.; Shao, Q.; Song, J.; Hu, Q.; Naik, N.; Guo, Z. Advances in waterborne acrylic resins: Synthesis principle, modification strategies, and their applications. *ACS Omega* **2021**, *6*, 2443–2449. [CrossRef]
11. González, E.; Stuhr, R.; Vega, J.M.; García-Lecina, E.; Grande, H.-J.; Leiza, J.R.; Paulis, M. Assessing the effect of CeO_2 nanoparticles as corrosion inhibitor in hybrid biobased waterborne acrylic direct to metal coating binders. *Polymers* **2021**, *13*, 848. [CrossRef]
12. Ecco, L.G.; Fedel, M.; Deflorian, F.; Becker, J.; Iversen, B.B.; Mamakhel, A. Waterborne acrylic paint system based on nanoceria for corrosion protection of steel. *Prog. Org. Coat.* **2016**, *96*, 19–25. [CrossRef]
13. Chimenti, S.; Vega, J.M.; García-Lecina, E.; Grande, H.-J.; Paulis, M.; Leiza, J.R. In-situ phosphatization and enhanced corrosion properties of films made of phosphate functionalized nanoparticles. *React. Funct. Polym.* **2019**, *143*, 104334. [CrossRef]
14. Liu, Q.; Zhang, J.; Liu, W.; Guo, F.; Pei, J.; Zhu, C.; Zhang, W. Preparation and characterization of self-healing microcapsules embedding waterborne epoxy resin and curing agent for asphalt materials. *Constr. Build. Mater.* **2018**, *183*, 384–394. [CrossRef]
15. Bao, Y.; Yan, Y.; Chen, Y.; Ma, J.; Zhang, W.; Liu, C. Facile fabrication of BTA@ZnO microcapsules and their corrosion protective application in waterborne polyacrylate coatings. *Prog. Org. Coat.* **2019**, *136*, 105233. [CrossRef]
16. Njoku, C.N.; Bai, W.; Arukalam, I.O.; Yang, L.; Hou, B.; Njoku, D.I.; Li, Y. Epoxy-based smart coating with self-repairing polyurea-formaldehyde microcapsules for anticorrosion protection of aluminum alloy AA2024. *J. Coat. Technol. Res.* **2020**, *17*, 797–813. [CrossRef]
17. Ress, J.; Martin, U.; Bosch, J.; Bastidas, D.M. pH-triggered release of $NaNO_2$ corrosion inhibitors from novel colophony microcapsules in simulated concrete pore solution. *ACS Appl. Mater. Interfaces* **2020**, *12*, 46686–46700. [CrossRef] [PubMed]
18. Ramasubramanian, M.; Haran, B.S.; Popova, S.; Popov, B.N.; Petrou, M.F.; White, R.E. Inhibiting action of calcium nitrite on carbon steel rebars. *J. Mater. Civ. Eng.* **2001**, *13*, 10–17. [CrossRef]
19. Garcés, P.; Saura, P.; Zornoza, E.; Andrade, C. Influence of pH on the nitrite corrosion inhibition of reinforcing steel in simulated concrete pore solution. *Corros. Sci.* **2011**, *53*, 3991–4000. [CrossRef]
20. Söylev, T.A.; Richardson, M.G. Corrosion inhibitors for steel in concrete: State-of-the-art report. *Constr. Build. Mater.* **2008**, *22*, 609–622. [CrossRef]
21. Cánovas, M.F.; Selv, N.H.; Kawiche, G.M. Influence on the physical-mechanical properties of portland-cement mortar, have admixtures of colophony and tannin. *Mater. Construct.* **1989**, *216*, 15–22. [CrossRef]
22. Tu, F.; Lee, D. Controlling the stability and size of double-emulsion-templated poly(lactic-co-glycolic) acid microcapsules. *Langmuir* **2012**, *28*, 9944–9952. [CrossRef] [PubMed]
23. Ding, S.; Serra, C.A.; Vandamme, T.F.; Yu, W.; Anton, N. Double emulsions prepared by two–step emulsification: History, state-of-the-art and perspective. *J. Control. Release* **2019**, *295*, 31–49. [CrossRef] [PubMed]
24. Lu, F.; Song, B.; He, P.; Wang, Z.; Wang, J. Electrochemical impedance spectroscopy (EIS) study on the degradation of acrylic polyurethane coatings. *RSC Adv.* **2017**, *7*, 13742–13748. [CrossRef]
25. Ren, F.; Zheng, Y.-F.; Liu, X.-M.; Yue, X.-Y.; Ma, L.; Li, W.-G.; Lai, F.; Liu, J.-L.; Guan, W.-L. An investigation of the oxidation mechanism of abietic acid using two-dimensional infrared correlation spectroscopy. *J. Mol. Struct.* **2015**, *1084*, 236–243. [CrossRef]
26. Gao, F.; Du, A.; Ma, R.; Lv, C.; Yang, H.; Fan, Y.; Zhao, X.; Wu, J.; Cao, X. Improved corrosion resistance of acrylic coatings prepared with modified MoS_2 nanosheets. *Colloids Surf. A Physicochem. Eng. Asp.* **2020**, *587*, 124318. [CrossRef]
27. Andrade, C. Evaluation of the degree of carbonation of concretes in three environments. *Constr. Build. Mater.* **2020**, *230*, 116804. [CrossRef]
28. Mehta, P.K.; Monteiro, P.J. *Concrete: Microstructure, Properties, and Materials*, 4th ed.; McGraw-Hill Education: New York, NY, USA, 2014.
29. Brug, G.J.; Van den Eeden, A.L.G.; Sluyters-Rehbach, M.; Sluyters, J.H. The analysis of electrode impedances complicated by the presence of a constant phase element. *J. Electroanal. Chem. Interf. Electrochem.* **1984**, *176*, 275–295. [CrossRef]
30. Lewis, O.D.; Critchlow, G.W.; Wilcox, G.D.; de Zeeuw, A.; Sander, J. A study of the corrosion resistance of a waterborne acrylic coating modified with nano-sized titanium dioxide. *Prog. Org. Coat.* **2012**, *73*, 88–94. [CrossRef]